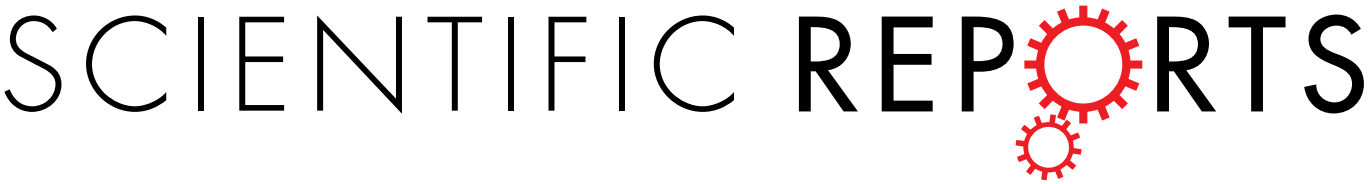

OPEN

Scattering of nanowire surface plasmons coupled to quantum dots with azimuthal angle difference

Received: 09 August 2016
Accepted: 01 November 2016
Published: 28 November 2016

Po-Chen Kuo[1], Guang-Yin Chen[2] & Yueh-Nan Chen[1,3]

Coherent scatterings of surface plasmons coupled to quantun dots have attracted great attention in plasmonics. Recently, an experiment has shown that the quantum dots located nearby a nanowire can be separated not only in distance, but also an angle ϕ along the cylindrical direction. Here, by using the real-space Hamiltonian and the transfer matrix method, we analytically obtain the transmission/reflection spectra of nanowire surface plasmons coupled to quantum dots with an azimuthal angle difference. We find that the scattering spectra can show completely different features due to different positions and azimuthal angles of the quantum dots. When additionally coupling a cavity to the dots, we obtain the Fano-like line shape in the transmission and reflection spectra due to the interference between the localized and delocalized modes.

Surface plasmons (SPs), or surface plasmon polaritons (SPPs), are propagating excitations of charge-density waves associated with the electromagnetic fields along the interface between a metal and a dielectric medium[1–6]. Surface plasmons in metallic nanostructures possess many advantages, such as enhanced transmission through subwavelength apertures[7,8], amplification by stimulated emission of radiation[9,10], enhanced photoluminescence from quantum wells[11], enhanced fluorescence[12–15], and surface-enhanced Raman scattering[12,16]. Moreover, there are many potential applications such as subwavelength imaging[1,17,18], waveguiding devices below the diffraction limit[19,20], biosensing[21], and biological detection[22]. Therefore, designing and fabricating subwavelength optical devices using SPs[23] open up new horizons of the research in this field.

With the tunable luminescence properties, such as localized surface plasmon resonances (LSPRs)[24], plasmon-induced fluorescence enhancement[15], broad excitation spectra, narrow emission spectra, and size-dependent emission[25], quantum dot (QD) has recently attracted much attention for its ability to act as a photon detector[25] or being an excellent single photon source[26–28]. On the other hand, metallic nanowire (MNW) is also an important class of plasmonic nanostructure for the SPs[29–34], resonators[30], sub-diffraction limit plasmon wave[31], and plasmon lasers[10].

Owing to the numerous advantages of both QD and MNW, QD that couples to MNW has emerged as an appealing system for coherent single-photon transport[35] and long-range energy transfer with a high efficiency[36]. By the virtue of coherent transport, there are many extended applications, such as transistors[37], plasmonic nanolaser[38], quantum switch[39,40], single-photon source[41], biological sensing[42,43], and nanoantennas[44,45]. Furthermore, the hybrid systems with exciton-plasmon interaction can reveal the features of cavity quantum electrodynamics[46–51] and have applications in quantum information processing[5,52–55].

A variety of experimental[33,36,41,56–62] and theoretical works[9,35,39,40,42,47,48–51,63–77] have been focused on the photon transport properties in the NW-QD systems. Recently, an experiment has reported that two QDs located nearby the NW are separated not only with a distance d, but also with an angle ϕ along the azimuthal direction[60]. Therefore, the difference in the angles between the QDs should be taken into account when investigating the scattering properities[33,34,48,78].

In this work, we study the scattering spectra of the nanowire SPs coupled to double QDs with an azimuthal angle difference. We also consider the system comprising N QDs. Taking into account the angle difference between the dots, we study the scattrering properties of the SPs by using the transfer matrices. Compared to the double-dot case, we find the transmission/reflection profile reveals the periodic behavior for the three-dot case[58]

[1]Department of Physics, National Cheng-Kung University, Tainan 701, Taiwan. [2]Department of Physics, National Chung Hsing University, Taichung 402, Taiwan. [3]Physics Division, National Center for Theoretical Sciences, Hsinchu, Taiwan. Correspondence and requests for materials should be addressed to G.-Y.C. (email: gychen@phys.nchu.edu.tw) or Y.-N.C. (email: yuehnan@mail.ncku.edu.tw)

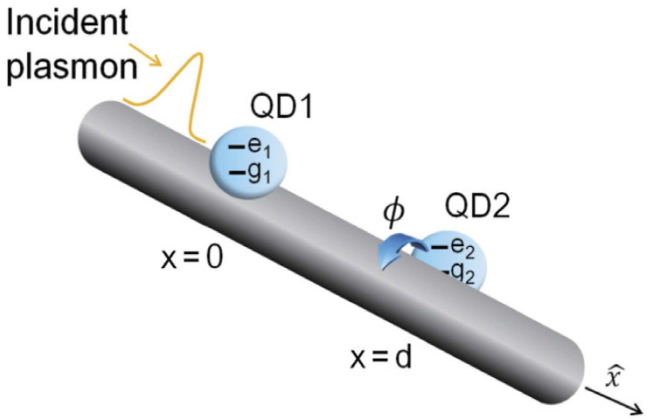

Figure 1. Schematic diagram of the two-QD model. Schematic diagram of the model: a metal nanowire coupled to two semiconductor QDs. A single surface plasmon injected from the left can be scattered by the two QDs which are placed on top of the nanowire with a inter-dot distance d along the $\hat{x}$ direction and an azimuthal angle ϕ along the $\hat{\varphi}$ direction.

when rotating each QD along $\hat{\varphi}$ direction. We further study the scattering spectra of the Hybrid Quantum System (HQS) consisting of QDs and a metal nanoparticle[79–81]. It can be viewed as a cavity[82–85] coupled to the NW-QD system. We find that the spectra reveal sharp and asymmetric response line shapes in the hybrid configuration. We analyze the results and provide explanations for the appearance of the Fano resonance.

Results

The Model. Lets us consider two identical QDs near a cylindrical metal nanowire. Assuming that they have the same separation from the metal wire, both with energy spacing $\hbar\omega_0$, separated not only with a distance d, but also with an angle ϕ as shown in Fig. 1. Since the propagating modes are along the $\hat{x}$ and $\hat{\varphi}$ directions, the phase differences acquired by the second dot are ikx and $in\phi$, where k and n are the wave number and quantum number governing the x and φ components, respectively. Under the rotating wave approximation, the interactions between the propagating photons and quantum dots can be described by the Hamiltonian,

$$\begin{aligned} \mathrm{H} &= \hbar\sum_{j=1,2}\left[\omega_0 - i\left(\frac{\Gamma'}{2}\right)\right]\sigma_{e_j e_j} + \sum_n\int dk\hbar v_g|k|a^\dagger_{k,n}a_{k,n} \\ &\quad - \hbar g\sum_n\int dk\,[(\sigma^{(1)}_+ + \sigma^{(2)}_+ e^{ikd}e^{in\phi})a_{k,n} + H.\,c.], \end{aligned} \tag{1}$$

where $\sigma_{e_j e_j} = |e_j\rangle\langle e_j|$ represents the diagonal element of the j^{th} QD operator with a atomic resonance frequency ω_0 and $\sigma^{(j)}_+ = |e_j\rangle\langle g_j|$ represents the rasing operator. Here, $a^\dagger_{k,n}$ ($a_{k,n}$) is the creation (annihilation) operator of the SP. We assume a SP is incident from the left with energy $E_k = v_g k$ for the n^{th} mode. Here, v_g and k are the group velocity and wave number of the incident SP, respectively. Since the SPs are confined on the surface of the cylindrical nanowire, the summation of n in Eq. (1) stands for the contributions from all the possible n modes, and g is the coupling constant between the SP and QD exciton. Note that $\Gamma' \equiv \gamma_0 + \Gamma_0$ is the total dissipation including the decay rate into free space γ_0 and other dissipative channels Γ_0. By using the Fourier transform, each term in Eq. (1) can be easily represented in real space

$$\begin{aligned} \mathrm{H} &= \hbar\iint dxd\varphi\Big\{-iv_g C^\dagger_R(x,\varphi)\frac{\partial}{\partial x}C_R(x,\varphi) + iv_g C^\dagger_L(x,\varphi)\frac{\partial}{\partial x}C_L(x,\varphi) \\ &\quad + \hbar g\sum_{j=1,2}\delta(x-(j-1)d)\delta(\varphi-(j-1)\phi) \\ &\quad [C^\dagger_R(x,\varphi)\sigma^{(j)}_- + C_R(x,\varphi)\sigma^{(j)}_+ + C^\dagger_L(x,\varphi)\sigma^{(j)}_- + C_L(x,\varphi)\sigma^{(j)}_+]\Big\} \\ &\quad + \hbar\sum_{j=1,2}\left[\omega_0 - i\left(\frac{\Gamma'}{2}\right)\right]\sigma_{e_j e_j}, \end{aligned} \tag{2}$$

where $C^\dagger_R(x,\varphi)[C^\dagger_L(x,\varphi)]$ is a bosonic operator creating a right-going (left-going) SP at x and φ. The stationary state of the above QDs-NW coupled system with the energy matching condition $E_k = v_g k$ can be written as

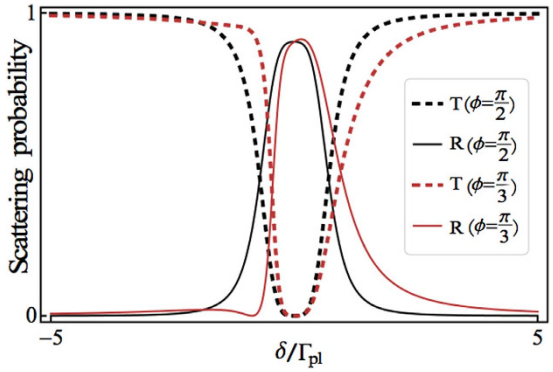

Figure 2. Effect from azimuthal angle difference in transmission spectra. The transmission probabilities $|t|^2$ (dashed line) and reflection probabilities $|r|^2$ (solid line) of the surface plasmon scattered by two QDs with azimuthal angle diference as a function of detuning $\delta \equiv \frac{E_k}{\hbar} - \omega_0$. When $d=0$ (here, it means the inter-dot distance is very small compared with the wavelength of incident fields), the two QDs are assumed to be at the same position.

$$\begin{aligned} |\mathbf{E}_k\rangle &= \int\int dxd\varphi[\psi^+_{k,n,R}C^\dagger_R(x,\varphi) + \psi^+_{k,n,L}C^\dagger_L(x,\varphi)]|g_1,g_2\rangle|0\rangle_{sp} \\ &+ \sum_{j=1,2}\xi_{k_j}\sigma^{(j)}_+|g_1,g_2\rangle|0\rangle_{sp}, \end{aligned} \tag{3}$$

where $|g_1, g_2\rangle\,|0\rangle_{sp}$ denotes that both the QDs are in their ground states with zero SP state, and ξ_{k_j} is the probability amplitude that the j^{th} QD jumps to its excited state. Suppose that a SP is incident from the left, the scattering amplitudes $\psi^+_{k,n,R}$ and $\psi^+_{k,n,L}$ take the forms

$$\begin{aligned} \psi^+_{k,n,R} &\equiv e^{ikx}e^{in\varphi}[\theta(-x) + a\theta(x)\theta(d-x) + t\theta(x-d)], \\ \psi^+_{k,n,L} &\equiv e^{-ikx}e^{-in\varphi}[r\theta(-x) + b\theta(x)\theta(d-x)], \end{aligned} \tag{4}$$

where t and r are the transmission and reflection amplitude, respectively. Here, a and b represent the probability amplitudes of the SP between $x=0$ and d, $\varphi=0$ and ϕ, respectively. Besides, $\theta(x)$ is the unit step function. From the eigenvalue equation, $H|\mathbf{E}_k\rangle = E_k|\mathbf{E}_k\rangle$, one can obtain the following relations for the coefficients:

$$\begin{aligned} a &= 1 + \frac{g}{iv_g}\xi_{k_1},\ b = \frac{g}{iv_g}\xi_{k_2}e^{i(kd+n\phi)}, \\ t &= 1 + \frac{g}{iv_g}\left[\xi_{k_1} + \xi_{k_2}e^{-i(kd+n\phi)}\right], \\ r &= \frac{g}{iv_g}\left[\xi_{k_1} + \xi_{k_2}e^{i(kd+n\phi)}\right], \\ \left(\delta + i\frac{\Gamma'}{2}\right)\xi_{k_1} &= 2g\left\{1 + \frac{g}{iv_g}\left[\xi_{k_1} + \xi_{k_2}e^{i(kd+n\phi)}\right]\right\}, \\ \left(\delta + i\frac{\Gamma'}{2}\right)\xi_{k_2} &= 2g\left[\left(1 + \frac{g}{iv_g}\right)\xi_{k_1}e^{i(kd+n\phi)} + \frac{g}{iv_g}\xi_{k_2}\right], \end{aligned} \tag{5}$$

where $\delta \equiv \frac{E_k}{\hbar} - \omega_0$ is the detuning between the incident SP energy with E_k and the QD exciton energy ω_0. By solving Eq. (5), the exact forms of the transmission and reflection amplitudes, t and r, are given by

$$\begin{aligned} t &= \frac{F^2}{(F+1)^2 - e^{2i(kd+n\phi)}}, \\ r &= \frac{(F+1) + (F-1)e^{2i(kd+n\phi)}}{e^{2i(kd+n\phi)} - (F+1)^2}. \end{aligned} \tag{6}$$

Here, we have defined the function $F \equiv \left(\frac{\gamma_0}{\Gamma_{pl}} + \frac{\Gamma_0}{\Gamma_{pl}}\right) - \frac{2i\delta}{\Gamma_{pl}}$, where $\Gamma_{pl} = \frac{4\pi g^2}{v_g}$ is the decay rate into the SP modes. The transmission and reflection probabilities of the SP are defined as $T=|t|^2$ and $R=|r|^2$, respectively, as shown in Fig. 2.

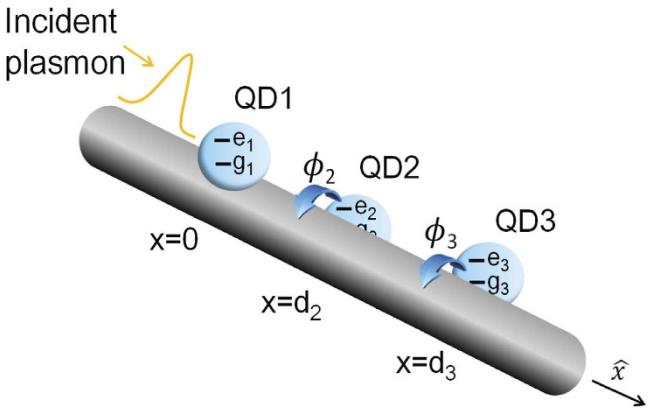

Figure 3. Schematic diagram of the three-QD model. Schematic diagram of the three QDs coupled to a metal nanowire with azimuthal angle difference along the $\hat{\varphi}$ direction.

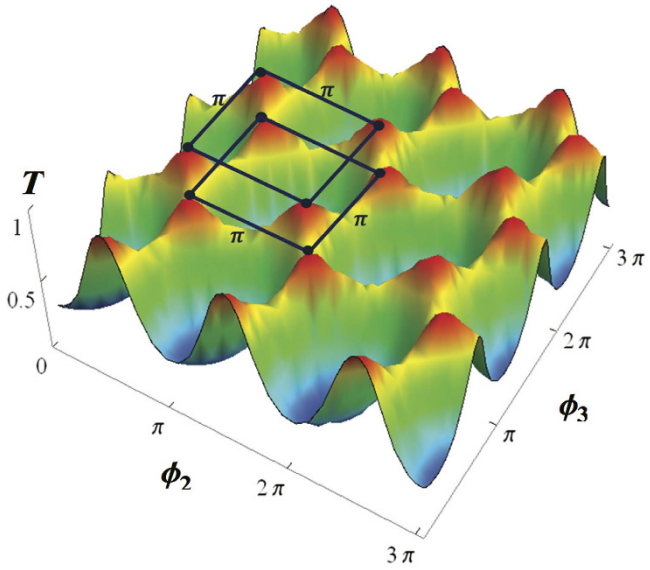

Figure 4. The interference of the azimuthal differences for the three-QD case. Analysis of the scattering probabilities of three quantum dots with the azimuthal angle differences between the second QD (ϕ_2) and third QD (ϕ_3) for the mode $n=1$, $k=1$, $d_2=\pi$, $d_3=2\pi$ and $\delta/\Gamma_{pl}=1$. Here, the red regions indicate the high transmission probability around unity.

Plasmon Scattered By N Quantum Dots. We now consider further a general model consisting of N identical QDs coupled to the SP. Under the rotating wave approximation, the interaction Hamiltonian becomes

$$\begin{aligned} \mathrm{H} &= \hbar \iint dx d\varphi \Big\{ -iv_g C_R^{\dagger}(x,\varphi)\frac{\partial}{\partial x}C_R(x,\varphi) + iv_g C_L^{\dagger}(x,\varphi)\frac{\partial}{\partial x}C_L(x,\varphi) \\ &+ \hbar g \sum_{j=1}^{N}\sum_{\lambda=R,L}\delta(x-d_{(j)})\delta(\varphi-\phi_j)\Big[C_\lambda^{\dagger}(x,\varphi)\sigma_-^{(j)} + C_\lambda(x,\varphi)\sigma_+^{(j)}\Big]\Big\} \\ &+ \hbar\sum_{j=1}^{N}\left[\omega_0 - i\left(\frac{\Gamma'}{2}\right)\right]\sigma_{e_j e_j}, \end{aligned} \tag{7}$$

where $d_{(j)}$ is the distance between the first dot and j^{th} dot, and ϕ_j is the angle of j^{th} QD with respect to the first QD along the $\hat{\varphi}$ direction when setting d_1 and ϕ_1 being zero. On the other hand, the scattering property of a nanowire coupled to N identical QDs can also be studied by applying the transfer-matrix method. Let us briefly review the transmission amplitude t and the reflection amplitude r for the case of a single-dot coupled to the nanowire:

$$t = \frac{F}{F+1}, r = \frac{-1}{F+1}, \tag{8}$$

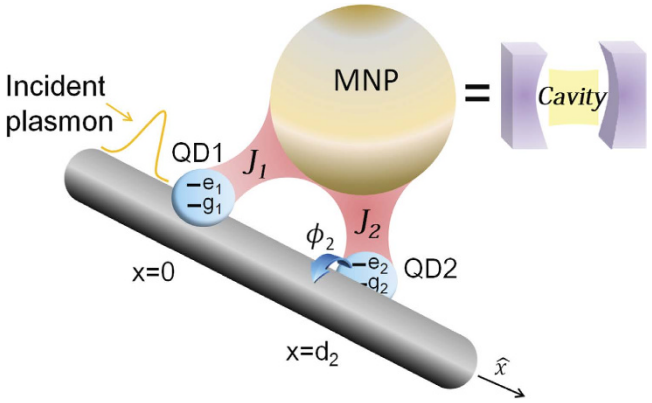

Figure 5. Schematic diagram of the QD-wire-nanoparticle hybrid system. Schematic diagram of the hybrid quantum system comprising QDs-wire and metal nanoparticle. The coupling strengths between the metal nanoparticle and QD-1, QD-2 are J_1 and J_2, respectively. The metal nanoparticle can be viewed as a special "cavity" in the strong coupling regime.

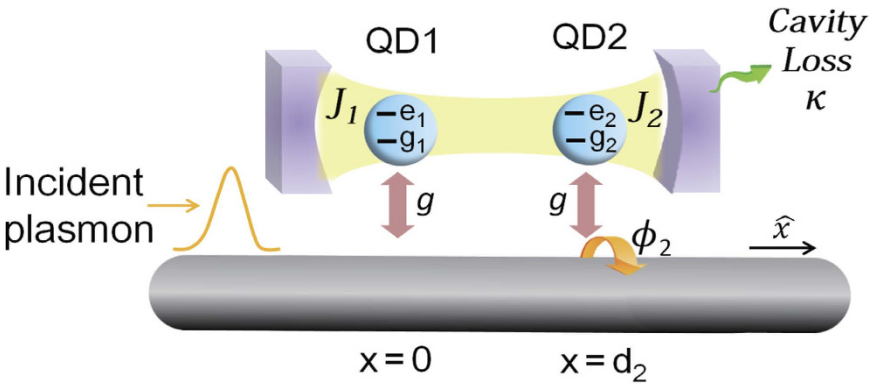

Figure 6. Schematic sketch of the effective hybrid model: common cavity. Schematic sketch of the effective hybrid model. Both QD-1 and QD-2 are coupled to a common cavity with a loss rate κ of the cavity photons. The transmission spectrum shows the Fano lineshape due to the interference between different channels. Here, the coupling strengths between cavity and QD-1, QD-2 are J_1 and J_2, respectively.

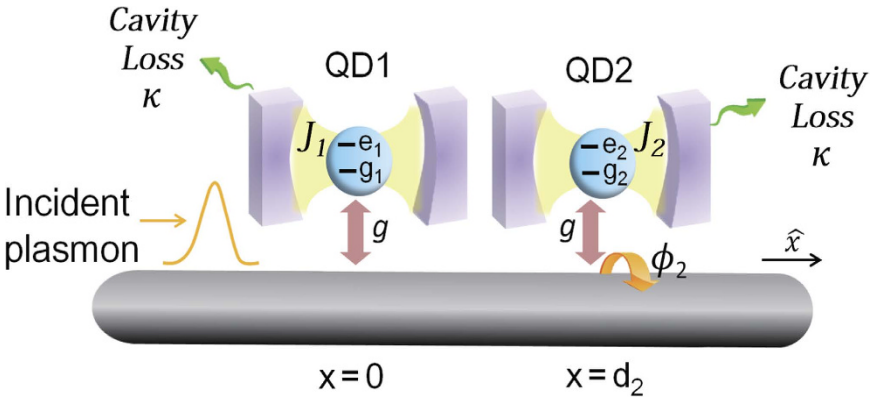

Figure 7. Schematic sketch of the effective hybrid model: individual cavity. Schematic draw of the model for each QD is individually coupled to different cavities with the same loss rate κ of the cavity photons.

where F has been defined in Sec. II. By making use of the transmission and reflection coefficients in Eq. (8), the transfer matrix T_q of the NW coupled to a single-QD can be written as

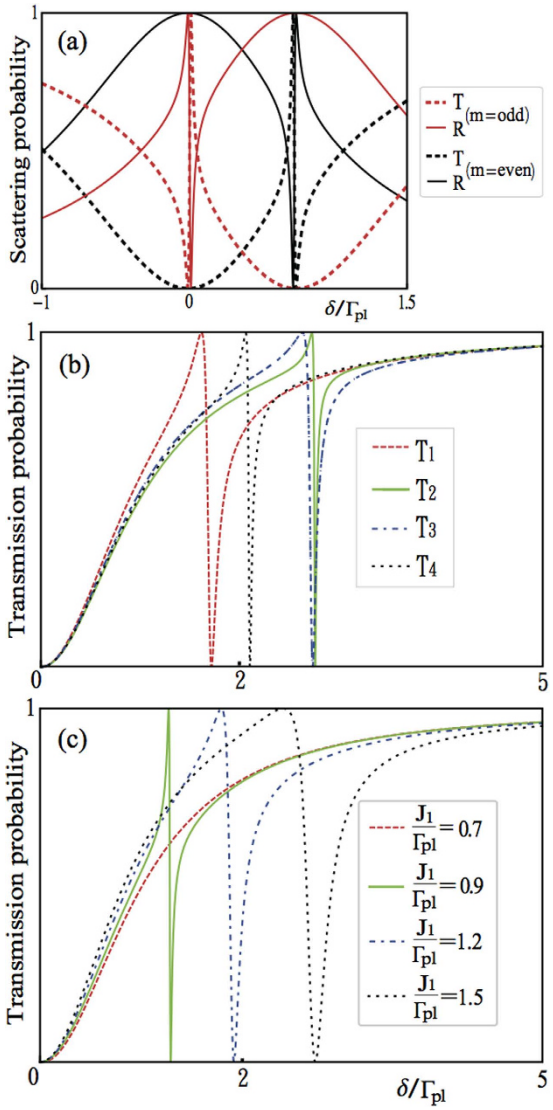

Figure 8. Scattering spectra for the two QDs coupled to common nanoparticle. (**a**) The transmission (dashed) and reflection (solid) probabilities as a function of detuning $\epsilon/\Gamma_{pl} = 1, \Im_1 = 0.5$ and $\Im_2 = 0.7$ when $kd_1 + n\phi_2 = m\pi$ with m being an odd (red) or even (black) integer. (**b**) When m is an odd integer and $\Im_1$ is close to $\Im_2$ with appropriate value of ϵ/Γ_{pl}, the typical transmission spectra present more distinct Fano resonance for the first case. For $\Gamma' = 0$ and $\kappa = 0$, we plot the transmission probabilities T_1(red-dashed), T_2(green-solid), T_3(blue-dot-dashed), T_4(black-dotted) with the detuning $\epsilon/\Gamma_{pl} = 0.05, 0.6, 1.2, 3$ when $\Im_1 = 0.25, 1, 1.5, 2$, $\Im_2 = 0.15, 0.8, 1, 1.5$, respectively. (**c**) The transmission probabilities T as a function of $\epsilon/\Gamma_{pl} = 1, \Im_2 = 0.7$ for $\Gamma' = 0$ and $\kappa = 0$ when $\Im_1 = 0.7, 0.9, 1.2, 1.5$, respectively.

$$T_q = \frac{1}{t}\begin{bmatrix} t^2 - r^2 & r \\ -r & 1 \end{bmatrix} = \frac{1}{F}\begin{bmatrix} F-1 & -1 \\ 1 & F+1 \end{bmatrix}. \tag{9}$$

Thus, the transfer matrix τ for the entire system is determined by

$$\tau = \prod_{j=1}^{N} T_{q_j} T_{d_j\phi_j}, \tag{10}$$

where

$$T_{d_j\phi_j} = \begin{bmatrix} e^{i\chi} & 0 \\ 0 & e^{-i\chi} \end{bmatrix} \tag{11}$$

represents the transfer matrix of free propagation with $\chi \equiv k[d_{(j)} - d_{(j-1)}] + n[\phi_j - \phi_{(j-1)}]$. Consequently, the total reflect and transmit amplitudes with N QDs can be obtained:

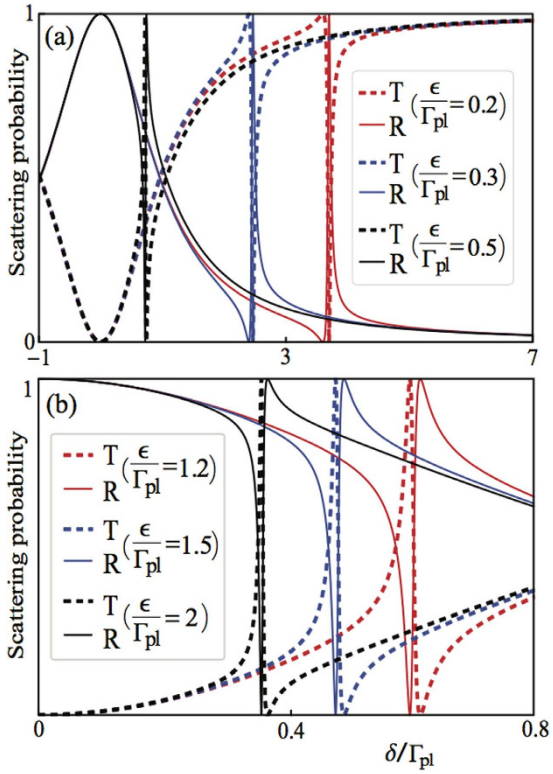

Figure 9. Analysis of Fano resonance. The transmission (dashed) and reflection (solid) probabilities as a function of $\mathfrak{J}_1 = 0.5, \mathfrak{J}_2 = 0.7$ for $\Gamma' = 0$ and $\kappa = 0$ when (**a**) $\epsilon/\Gamma_{pl} = 0.2, 0.3, 0.5$, (**b**) $\epsilon/\Gamma_{pl} = 1.2, 1.5, 2$, respectively. The position of the Fano lineshape can be shifted from the right to the left along the δ/Γ_{pl} axis when increasing the detuning ϵ/Γ_{pl}.

$$\begin{bmatrix} t_N \\ 0 \end{bmatrix} = \begin{bmatrix} e^{-i[kd_N + n\phi_N]} & 0 \\ 0 & 1 \end{bmatrix} \tau \begin{bmatrix} 1 \\ r_N \end{bmatrix}. \tag{12}$$

In order to make a comparison to the double-dot case, we specifically consider the three-dot case[58] as shown in Fig. 3. By solving the eigenvalue equation with $N = 3$ in Eq. (7) or Eq. (12), the transmission and reflection amplitudes can be obtained. For simplicity, we only show the transmission amplitudes

$$t = \frac{-F^3 e^{i\zeta}}{(F-1)e^{i\alpha} + (F+1)(e^{i\beta} + e^{i\gamma}) - (F+1)^3 e^{i\zeta}}, \tag{13}$$

where we have defined the phase terms $\zeta \equiv 2n\phi_2$, $\alpha \equiv 2[kd_3 + n(\phi_2 + \phi_3)]$, $\beta \equiv 2(kd_2 + 2n\phi_2)$ and $\gamma \equiv 2[k(d_3 - d_2) + n\phi_3]$, respectively. Here, we are interested in the scattering spectra resulting from the varying angles of QD-2 and QD-3. Figure 4 shows the scattering spectra as functions of the angles ϕ_2 and ϕ_3. We find that the transmission (reflection) coefficient reveals the periodic maximum (minimum) value 1 (0), when keeping one QD fixed at the certain angle along the $\hat{\varphi}$ direction.

QDs-NW System Coupled To Cavity. Recently, hybrid quantum system (HQS) has attracted renewed attention for its prospect of applications in future quantum devices. Here, we consider the HQS of the QDs (with nanowire) coupled to a metal-nanoparticle (MNP) as shown in Fig. 5. it was reported[82–87] that, for the very small separation between a quantum emitter and a metal nanoparticle, the spectral density of the surface electromagnetic fields of the nanoparticle becomes Lorentzian. This indicates that the emitter-nanoparticle system can form an effective cavity quantum electrodynamics (QED) system. We therefore study the scattering spectra of two kinds of HQS comprising the cavity coupled to two QDs. For the first case, we assume both QD-1 and QD-2 are coupled to the same cavity as shown in Fig. 6. In real space, the Hamiltonian of the cavity photon with a loss rate κ can be written as

$$H_S = H + \hbar\left[\omega_c - i\left(\frac{\kappa}{2}\right)\right]\sigma_{e_c e_c} + \sum_{j=1,2} J_j(\sigma_+^{(j)} a_c + \sigma_-^{(j)} a_c^\dagger), \tag{14}$$

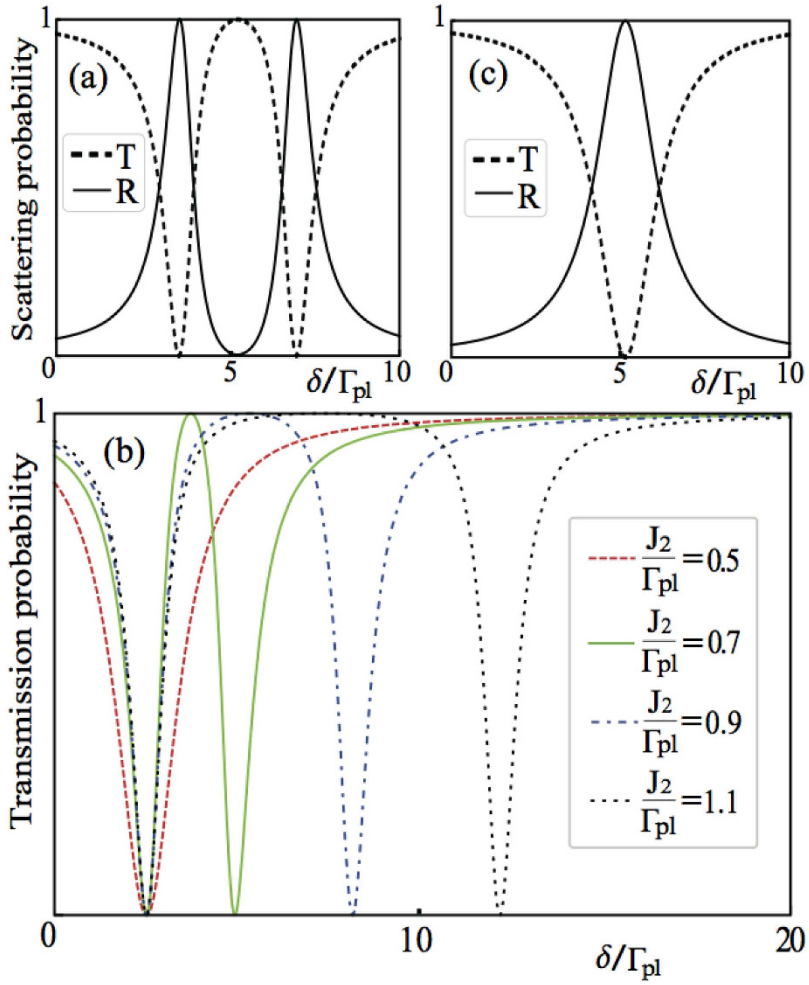

Figure 10. Scattering spectra for the two QDs coupled to individual nanoparticles. For the second case, we set $\Im_1 = 0.5$, $\Gamma' = \kappa = 0$, and $kd_1 + n\phi_2 = m\pi$ with m being an integer. (**a**) The transmission (dashed) and reflection (solid) probabilities as a function of $\Im_2 = 0.7$ and $\epsilon/\Gamma_{pl} = 0.07$. This panel shows a standard Breit-Wigner lineshape without the Fano resonance for two QDs. (**b**) The transmission probabilities as a function for $\Im_2 = 0.5$ (red-dashed), 0.7 (green-solid), 0.9 (blue-dot-dashed), 1.1 (black-dotted), respectively with $\epsilon/\Gamma_{pl} = 0.1$. By adjusting coupling strength between each QD to the cavity, the position of each peak along the δ/Γ_{pl} axis can be controlled. (**c**) When $\Im_1 = \Im_2 = 0.6$, the overlap of two peaks makes the two QDs act like a single QD in transmission(dashed) and reflection(solid) probabilities with $\epsilon/\Gamma_{pl} = 0.07$.

where $\sigma_{e_c e_c} = |e_c\rangle\langle e_c|$ is the diagonal element of the cavity operator, and $a_c^\dagger$ (a_c) is the bosonic creation(annihilation) operator of the cavity mode. Here, J_j represents the coupling strength between the cavity and j^{th} QD. The transmission and reflection coefficients can be written as

$$\begin{aligned} t &= \frac{-F[FG + 4(\Im_1^2 + \Im_2^2)] + 8i\Im_1\Im_2 \sin\varsigma}{e^{2i\varsigma}G + 8e^{i\varsigma}\Im_1\Im_2 - (F+1)[(F+1)G + 4(\Im_1^2 + \Im_2^2)]}, \\ r &= \frac{G[(F+1) + e^{2i\varsigma}(F-1)] + 4(\Im_2 - \Im_1 e^{i\varsigma})^2}{e^{2i\varsigma}G + 8e^{i\varsigma}\Im_1\Im_2 - (F+1)[(F+1)G + 4(\Im_1^2 + \Im_2^2)]}. \end{aligned} \tag{15}$$

Here, we have defined the function $G \equiv (\kappa - 2i\epsilon)/\Gamma_{pl}$, $\Im_1(\Im_2) \equiv J_1/\Gamma_{pl}(J_2/\Gamma_{pl})$, and the phase term $\varsigma \equiv (kd_1 + n\phi_2)$. The detuning between the incident SP energy (with E_k) and the cavity resonant frequency (ω_c) is labeled by the symbol ε. For the second case, we study the configuration that each QD is individually coupled to its own cavity as shown in Fig. 7. Here, we have assumed the two cavities are identical for simplicity. The Hamiltonian of the composite system can be rewritten as

$$H_I = H + \hbar\sum_{i=1,2}\left[\omega_c - i\left(\frac{\kappa}{2}\right)\right]\sigma_{e_{c_i}e_{c_i}} + \sum_{j=1,2} J_j(\sigma_+^{(j)}a_{c_j} + \sigma_-^{(j)}a_{c_j}^\dagger), \tag{16}$$

where $\sigma_{e_{c_i}e_{c_i}}$ represents the diagonal element of the i^{th} cavity operator, and $a^{\dagger}_{c_j}(a_{c_j})$ is the bosonic creation(annihilation) operator of the j^{th} cavity mode. Also, the scattering coefficients can be obtained by solving eigenvalue equation:

$$\begin{aligned} t &= \frac{-(FG+4\mathfrak{J}_1^2)(FG+4\mathfrak{J}_2^2)}{[e^{2i\varsigma}-(F+1)^2]G^2-4G(F+1)(\mathfrak{J}_1^2+\mathfrak{J}_2^2)-16\mathfrak{J}_1^2\mathfrak{J}_2^2}, \\ r &= \frac{G\{e^{2i\varsigma}[(F-1)G+4\mathfrak{J}_1^2]+G(F+1)+4\mathfrak{J}_2^2\}}{[e^{2i\varsigma}-(F+1)^2]G^2-4G(F+1)(\mathfrak{J}_1^2+\mathfrak{J}_2^2)-16\mathfrak{J}_1^2\mathfrak{J}_2^2}, \end{aligned} \tag{17}$$

We plot in Figs 8, 9 and 10 the transmission probabilities $T=|t|^2$ (dashed lines) and reflection probabilities $R=|r|^2$ (solid lines) as a function of the detuning for the both cases. In plotting Fig. 8, we find that when $kd_1+n\phi_2=\pi m$ with m being an integer and $\mathfrak{J}_1$ being close to $\mathfrak{J}_2$ with appropriate value of ϵ/Γ_{pl}, the transmission and reflection spectra have a more distinct Fano-type line shapes. In Fig. 9, when increasing the detuning ϵ/Γ_{pl}, the position of the Fano-type line shapes would be shifted from the right to the left along the δ/Γ_{pl} axis. For the second case, however, we can only observe two peaks with the absence of asymmetric Fano-type line shape as shown in Fig. 10. When increasing the detuning ϵ, the inter-peak separation is reduced rapidly.

Discussion

Since the Fano resonance only occurs in the first case, it is interesting to ask: What makes the two cases different? To answer this, let us note that, in Fig. 8(b), the stronger coupling strength of the two QDs to the cavity, the larger detuning ϵ is required to form the Fano-type line shapes for the first case. Contrarily, when J_1 coincides with J_2, the Fano resonance vanishes rapidly. In this regard, the Fano resonance arises from the constructive and destructive interference between the localized and delocalized channels by the virtue of the coupling of the two QDs to the same cavity. Here, the localized channel represents the single QD mode, and the delocalized channel denotes the hybridization mode of the cavity photon and the two dots[88]. The surface plasmons passing through the two channels carry different phases and result in the interference. On the other hand, we can easily control the position of each peak along the δ/Γ_{pl} axis by adjusting the coupling strength between each QD to the cavity in the second case as shown in Fig. 10. When $J_1=J_2$, the overlapping of two peaks makes the two QDs collectively act like a single QD. The notable feature of these results indicates that the Fano-type line shape can't be created due to the individual coupling to each own cavity. In other words, the difference between J_1 and J_2 is the primary cause of the Fano resonance.

In conclusion, the real-space Hamiltonians and transfer-matrix method are used to obtain the transport properties of SPs propagating on the surface of a silver NW coupled to QDs. The transmission and reflection spectra of the SPs depend not only on the position, but also on the azimuthal angle of the QDs. For the double-dot case, even the two QDs are placed at the same position in the $\hat{x}$-axis, changing the angle of a QD along $\hat{\varphi}$ direction also affects the reflection (transmission) spectra. For the triple-dot case, the transmission (reflection) coefficient reveals the periodic maximum (minimum) value when keeping one QD fixed at the certain angle along the $\hat{\varphi}$ direction. Moreover, when there is an additional cavity coupled to QDs, the Fano-type line shape can be created if both the QDs are coupled to the same cavity. The appearance of Fano resonances is attributed to the interference between the localized and delocalized modes.

References

1. Zayats, A. V., Smolyaninov, I. I. & Maradudin, A. A. Nano-optics of surface plasmon polaritons. *Physics Reports* **408,** 131–314 (2005).
2. Zayats, A. V. & Smolyaninov, I. I. Near-field photonics: surface plasmon polaritons and localized surface plasmons. *Journal of Optics A: Pure and Applied Optics* **5,** S16–S50 (2003).
3. Bliokh, K. Y., Smirnova, D. & Nori, F. Quantum spin Hall effect of light. *Science* **348,** 1448–1451 (2015).
4. Bliokh, K. Y., Rodrguez-Fortuño, F. J., Nori, F. & Zayats, A. V. Spin-orbit interactions of light. *Nature Photonics* **9,** 796808 (2015).
5. Antognozzi, M. *et al.* Direct measurements of the extraordinary optical momentum and transverse spin-dependent force using a nano-cantilever. *Nature Physics* **12,** 731–735 (2016).
6. Bliokh, K. Y. & Nori, F. Transverse and longitudinal angular momenta of light. *Physics Reports* **592,** 1–38 (2015).
7. Thio, T. *et al.* Enhanced light transmission through a single subwavelength aperture. *Opt. Lett.* **26,** 1972–1974 (2001).
8. Genet, C. & Ebbesen, T. W. Light in tiny holes. *Nature* **445,** 39–46 (2007).
9. Bergman, D. J. & Stockman, M. I. Surface plasmon amplification by stimulated emission of radiation: Quantum generation of coherent surface plasmons in nanosystems. *Phys. Rev. Lett.* **90,** 027402 (2003).
10. Oulton, R. F. *et al.* Plasmon lasers at deep subwavelength scale. *Nature* **461,** 629–632 (2009).
11. Hecker, N. E. *et al.* Surface plasmon-enhanced photoluminescence from a single quantum well. *Applied Physics Letters* **75,** 1577 (1999).
12. Nie, S. & Emory, S. R. Probing single molecules and single nanoparticles by surface-enhanced Raman scattering. *Science* **275,** 1102–1106 (1997).
13. Kühn, S., Håkanson, U., Rogobete, L. & Sandoghdar, V. Enhancement of single-molecule fluorescence using a gold nanoparticle as an optical nanoantenna. *Phys. Rev. Lett.* **97,** 017402 (2006).
14. Gu, Y., Huang, L., Martin, O. J. F. & Gong, Q. Resonance fluorescence of single molecules assisted by a plasmonic structure. *Phys. Rev. B* **81,** 193103 (2010).
15. Sadeghi, S. M., West, R. G. & Nejat, A. Photo-induced suppression of plasmonic emission enhancement of CdSe/ZnS quantum dots. *Nanotechnology* **22,** 405202 (2011).
16. Kneipp, K. *et al.* Single molecule detection using surface-enhanced Raman scattering. *Phys. Rev. Lett.* **78,** 1667–1670 (1997).
17. Klimov, V., Ducloy, M. & Letokhov, V. A model of an apertureless scanning microscope with a prolate nanospheroid as a tip and an excited molecule as an object. *Chemical Physics Letters* **358,** 192–198 (2002).
18. Smolyaninov, I. I., Elliott, J., Zayats, A. V. & Davis, C. C. Far-field optical microscopy with a nanometer-scale resolution based on the in-plane image magnification by surface plasmon polaritons. *Phys. Rev. Lett.* **94,** 057401 (2005).

19. Brongersma, M. L., Hartman, J. W. & Atwater, H. A. Electromagnetic energy transfer and switching in nanoparticle chain arrays below the diffraction limit. *Phys. Rev. B* **62,** R16356–R16359 (2000).
20. Bozhevolnyi, S. I. *et al.* Channel plasmon subwavelength waveguide components including interferometers and ring resonators. *Nature* **440,** 508–511 (2006).
21. Oldenburg, S. J., Genick, C. C., Clark, K. A. & Schultz, D. A. Base pair mismatch recognition using plasmon resonant particle labels. *Analytical Biochemistry* **309,** 109–116 (2002).
22. Schultz, D. A. Plasmon resonant particles for biological detection. *Current Opinion in Biotechnology* **14,** 13–22 (2003).
23. Chang, D. E., Sørensen, A. S., Hemmer, P. R. & Lukin, M. D. All-optical modulation by plasmonic excitation of CdSe quantum dots. *Nature Photonics* **1,** 402–406 (2007).
24. Luther, J. M., Jain, P. K., Ewers, T. & Alivisatos, A. P. Localized surface plasmon resonances arising from free carriers in doped quantum dots. *Nature Materials* **10,** 361–366 (2011).
25. Narayanaswamy, A., Feiner, L. F., Meijerink, A. & van der Zaag, P. J. The effect of temperature and dot size on the spectral properties of colloidal inp/zns coreshell quantum dots. *ACS Nano* **3,** 2539–2546 (2009).
26. Michler, P. *et al.* Quantum correlation among photons from a single quantum dot at room temperature. *Nature* **406,** 968–970 (2000).
27. Santori, C. *et al.* Triggered single photons from a quantum dot. *Phys. Rev. Lett.* **86,** 1502–1505 (2001).
28. Deshpande, S., Heo, J., Das, A. & Bhattacharya, P. Electrically driven polarized single-photon emission from an InGaN quantum dot in a GaN nanowire. *Nature Communication* **4,** 1675 (2012).
29. Dickson, R. M. & Lyon, L. A. Unidirectional plasmon propagation in metallic nanowires. *The Journal of Physical Chemistry B* **104,** 6095–6098 (2000).
30. Ditlbacher, H. *et al.* Silver nanowires as surface plasmon resonators. *Phys. Rev. Lett.* **95,** 257403 (2005).
31. Krenn, J. R. *et al.* Nondiffraction-limited light transport by gold nanowires. *Euro. Phys. Lett.* **60,** 663 (2002).
32. Sanders, A. W. *et al.* Observation of Plasmon Propagation, Redirection, and Fan-Out in Silver Nanowires. *Nano Letters* **6,** 1822–1826 (2006).
33. Wei, H. & Xu, H. Nanowire-based plasmonic waveguides and devices for integrated nanophotonic circuits. *Nanophotonics* **1,** 155–169 (2012).
34. Lal, S. *et al.* Noble metal nanowires: From plasmon waveguides to passive and active devices. *Accounts of Chemical Research* **45,** 1887–1895 (2012).
35. Cheng, M. T., Luo, Y. Q., Wang, P. Z. & Zhao, G. X. Coherent controlling plasmon transport properties in metal nanowire coupled to quantum dot. *Applied Physics Letters* **97,** 191903 (2010).
36. Zhou, Z. K. *et al.* Plasmon-mediated radiative energy transfer across a silver nanowire array via resonant transmission and subwavelength imaging. *ACS Nano* **4,** 5003–5010 (2010).
37. Chang, D. E., Sørensen, A. S., Demler, E. A. & Lukin, M. D. A single-photon transistor using nanoscale surface plasmons. *Nature Phys.* **3,** 807–812 (2007).
38. Tatebayashi, J. *et al.* Room-temperature lasing in a single nanowire with quantum dots. *Nature Photonics* **9,** 501–505 (2015).
39. Kim, N. C. *et al.* Switching of a single propagating plasmon by two quantum dots system. *Applied Physics Letters* **97,** 061110 (2010).
40. Zhou, L. *et al.* Quantum Zeno switch for single-photon coherent transport *Phys. Rev. A* **80,** 062109 (2009).
41. Akimov, A. V. *et al.* Generation of single optical plasmons in metallic nanowires coupled to quantum dots. *Nature* **450,** 402–406 (2007).
42. Cheng, M. T. & Song, Y. Y. Fano resonance analysis in a pair of semiconductor quantum dots coupling to a metal nanowire. *Opt. Lett.* **37,** 978–980 (2012).
43. Hatef, A., Sadeghi, S. M., Boulais, È. & Meunier, M. Quantum dot-metallic nanorod sensors via exciton-plasmon interaction. *Nanotechnology* **24,** 015502 (2013).
44. Curto, A. G. *et al.* Multipolar radiation of quantum emitters with nanowire optical antennas. *Nature Communications* **4,** 1750 (2013).
45. Kremer, P. E. *et al.* Strain-tunable quantum dot embedded in a nanowire antenna. *Phys. Rev. B* **90,** 201408 (2014).
46. Chang, D. E., Sørensen, A. S., Hemmer, P. R. & Lukin, M. D. Quantum optics with surface plasmons. *Phys. Rev. Lett.* **97,** 053002 (2006).
47. Chen, G. Y., Chen, Y. N. & Chuu, D. S. Spontaneous emission of quantum dot excitons into surface plasmons in a nanowire. *Opt. Lett.* **33,** 2212–2214 (2008).
48. Chen, Y. N., Chen, G. Y., Chuu, D. S. & Brandes, T. Quantum-dot exciton dynamics with a surface plasmon: Band-edge quantum optics. *Phys. Rev. A* **79,** 033815 (2009).
49. Chen, Y. N. *et al.* Detecting non-markovian plasmonic band gaps in quantum dots using electron transport. *Phys. Rev. B* **79,** 245312 (2009).
50. Zhou, L. *et al.* Quantum super-cavity with atomic mirrors. *Phys. Rev. A* **78,** 063827 (2008).
51. Liao, J. Q. *et al.* Controlling the transport of single photons by tuning the frequency of either one or two cavities in an array of coupled cavities *Phys. Rev. A* **81,** 042304 (2010).
52. Bouwmeester, D., Ekert, A. & Zeilinger, A. *The Physics of Quantum Information* (Springer, Berlin, 2000).
53. Reimer, M. E. *et al.* Bright single-photon sources in bottom-up tailored nanowires. *Nature Communications* **3,** 737 (2012).
54. Bliokh, K. Y., Bekshaev, A. Y. & Nori, F. Extraordinary momentum and spin in evanescent waves. *Nature Communications* **5,** 3300 (2014).
55. Bekshaev, A. Y., Bliokh, K. Y. & Nori, F. Transverse Spin and Momentum in Two-Wave Interference. *Phys. Rev. X* **5,** 011039 (2015).
56. Fedutik, Y. *et al.* Exciton-plasmon-photon conversion in plasmonic nanostructures. *Phys. Rev. Lett.* **99,** 136802 (2007).
57. Gruber, C., Kusar, P., Hohenau, A. & Krenn, J. R. Controlled addressing of quantum dots by nanowire plasmons. *Appl. Phys. Lett.* **100,** 231102 (2012).
58. Heiss, M. *et al.* Self-assembled quantum dots in a nanowire system for quantum photonics. *Nature Materials* **12,** 439–444 (2013).
59. Bulgarini, G. *et al.* Nanowire waveguides launching single photons in a gaussian mode for ideal fiber coupling. *Nano Letters* **14,** 4102–4106 (2014).
60. Li, Q., Wei, H. & Xu, H. Resolving single plasmons generated by multiquantum-emitters on a silver nanowire. *Nano Letters* **14,** 3358–3363 (2014).
61. Li, Q., Wei, H. & Xu, H. Quantum yield of single surface plasmons generated by a quantum dot coupled with a silver nanowire. *Nano Letters* **15,** 8181–8187 (2015).
62. Ropp, C. *et al.* Nanoscale probing of image-dipole interactions in a metallic nanostructure. *Nature Communications* **6,** 6558 (2015).
63. Rosenblit, M., Horak, P., Helsby, S. & Folman, R. Single-atom detection using whispering-gallery modes of microdisk resonators. *Phys. Rev. A* **70,** 053808 (2004).
64. Shen, J. T. & Fan, S. Coherent photon transport from spontaneous emission in one-dimensional waveguides. *Opt. Lett.* **30,** 2001–2003 (2005).
65. Bermel, P. *et al.* Single-photon all-optical switching using waveguide-cavity quantum electrodynamics. *Phys. Rev. A* **74,** 043818 (2006).
66. Zhou, L. *et al.* Controllable scattering of a single photon inside a one-dimensional resonator waveguide. *Phys. Rev. Lett.* **101,** 100501 (2008).
67. Shen, J. T. & Fan, S. Theory of single-photon transport in a single-mode waveguide. i. coupling to a cavity containing a two-level atom. *Phys. Rev. A* **79,** 023837 (2009).

68. Chen, W., Chen, G. Y. & Chen, Y. N. Coherent transport of nanowire surface plasmons coupled to quantum dots. *Opt. Express* **18,** 10360–10368 (2010).
69. Chen, G. Y. *et al.* Surface plasmons in a metal nanowire coupled to colloidal quantum dots: Scattering properties and quantum entanglement. *Phys. Rev. B* **84,** 045310 (2011).
70. Chen, W., Chen, G. Y. & Chen, Y. N. Controlling Fano resonance of nanowire surface plasmons. *Opt. Lett.* **36,** 3602–3604 (2011).
71. Chen, G. Y. & Chen, Y. N. Correspondence between entanglement and Fano resonance of surface plasmons. *Opt. Lett.* **37,** 4023–4025 (2012).
72. Barthes, J. *et al.* Coupling of a dipolar emitter into one-dimensional surface plasmon. *Scientific Reports* **3,** 2734 (2013).
73. Johansson, J. R. *et al.* Nonclassical microwave radiation from the dynamical Casimir effect. *Phys. Rev. A* **87,** 043804, 3 (2013).
74. Nation, P. D., Johansson, J. R., Blencowe, M. P. & Nori, F. Stimulating uncertainty: Amplifying the quantum vacuum with superconducting circuits. *Rev. Mod. Phys.* **84,** 1–24 (2012).
75. Johansson, J. R. *et al.* Observation of the dynamical Casimir effect in a superconducting circuit. *Nature* **479,** 376–379 (2011).
76. Johansson, J. R., Johansson, G., Wilson, C. M. & Nori, F. Dynamical Casimir effect in superconducting microwave circuits. *Phys. Rev. A* **82,** 052509 (2010).
77. Johansson, J. R., Johansson, G., Wilson, C. M. & Nori, F. Dynamical Casimir effect in superconducting microwave circuits. *Phys. Rev. Lett* **103,** 147003 (2009).
78. Huang, Y. *et al.* Nanowire-supported plasmonic waveguide for remote excitation of surface-enhanced Raman scattering. *Light: Science & Applications* **3,** e199 (2014).
79. Sadeghi, S. M. Tunable nanoswitches based on nanoparticle meta-molecules. *Nanotechnology* **21,** 355501 (2010).
80. Malyshev, A. V. & Malyshev, V. A. Optical bistability and hysteresis of a hybrid metal-semiconductor nanodimer. *Phys. Rev. B* **84,** 035314 (2011).
81. Li, J. B. *et al.* Optical bistability and nonlinearity of coherently coupled exciton-plasmon systems. *Opt. Express* **20,** 1856–1861 (2012).
82. Auffèves-Garnier, A., Simon, C., Gérard, J. M. & Poizat, J. P. Giant optical nonlinearity induced by a single two-level system interacting with a cavity in the purcell regime. *Phys. Rev. A* **75,** 053823 (2007).
83. Englund, D. *et al.* Controlling cavity reflectivity with a single quantum dot. *Nature* **450,** 857–861 (2007).
84. Chikkaraddy, R. *et al.* Single-molecule strong coupling at room temperature in plasmonic nanocavities. *Nature* **535,** 127–130 (2016).
85. Trügler, A. *Optical Properties of Metallic Nanoparticles* (Springer, Switzerland, 2016).
86. Delga, A., Feist, J., Bravo-Abad, J. & Garcia-Vidal, F. J. Quantum Emitters Near a Metal Nanoparticle: Strong Coupling and Quenching. *Phys. Rev. Lett* **112,** 253601 (2014).
87. González-Tudela, A. *et al.* Reversible dynamics of single quantum emitters near metal-dielectric interfaces. *Phys. Rev. B* **89,** 041402 (2014).
88. Luk'yanchuk, B. *et al.* The Fano resonance in plasmonic nanostructures and metamaterials. *Nature Materials* **9,** 707–715 (2010).

Acknowledgements

This work is supported partially by the National Center for Theoretical Sciences and Ministry of Science and Technology, Taiwan, grant number MOST 103-2112-M-006-017-MY4 and MOST 105-2112-M-005-008-MY3.

Author Contributions

Y.N.C. and G.Y.C. conceived the idea. P.C.K. carried out the calculations under the guidance of Y.N.C. and G.Y.C. All authors contributed to the interpretation of the work and the writing of the manuscript.

Additional Information

Competing financial interests: The authors declare no competing financial interests.

How to cite this article: Kuo, P.-C. *et al.* Scattering of nanowire surface plasmons coupled to quantum dots with azimuthal angle difference. *Sci. Rep.* **6**, 37766; doi: 10.1038/srep37766 (2016).

Publisher's note: Springer Nature remains neutral with regard to jurisdictional claims in published maps and institutional affiliations.